Journal of Solid State Chemistry 204 (2013) 298–304

Contents lists available at SciVerse ScienceDirect

Journal of Solid State Chemistry

journal homepage: www.elsevier.com/locate/jssc

Cyclic CO_2 chemisorption–desorption behavior of Na_2ZrO_3: Structural, microstructural and kinetic variations produced as a function of temperature

Lorena Martínez-dlCruz, Heriberto Pfeiffer *

Instituto de Investigaciones en Materiales, Universidad Nacional Autónoma de México, Circuito Exterior s/n Cd. Universitaria, Del. Coyoacán, CP 04510 México DF, Mexico

ARTICLE INFO

Article history:
Received 22 February 2013
Received in revised form
23 April 2013
Accepted 11 June 2013
Available online 21 June 2013

Keywords:
CO_2 capture
Cyclability
Sodium zirconate
Thermal analysis

ABSTRACT

A structural, microstructural and kinetic analysis of the Na_2ZrO_3–CO_2 system was performed over 20 chemisorption–desorption cycles. Different cyclic experiments were performed between 500 and 800 °C. Although the best results were obtained in Na_2ZrO_3 sample treated at 550 °C, all the samples treated between 500 and 700 °C presented good CO_2 chemisorption efficiencies and stabilities. On the contrary, Na_2ZrO_3 sample treated at 800 °C presented a continuous decrement of the CO_2 chemisorption. After 20 cycles all the samples presented a partial Na_2ZrO_3 decomposition, determined by the ZrO_2 formation, which was associated to sodium sublimation. Additionally, the Na_2ZrO_3 microstructural analysis showed a systematic morphological evolution. It was microscopically observed that Na_2ZrO_3 particles tend to fracture due to the Na_2CO_3 formation. Later, after several cycles these tiny fractured particles sinter producing new polyhedral and dense Na_2ZrO_3–ZrO_2 particles. Finally, an exhaustive kinetic analysis showed a high CO_2 chemisorption–desorption stability at different temperatures.

1. Introduction

In recent decades the greenhouse gas emissions have increased, which has led to an over warming of the earth. From these greenhouse gases, carbon dioxide (CO_2) approximately produces two-thirds of the overall warming [1]. For this reason, it has been proposed the CO_2 capture, where different alkaline ceramics have been studied as possible CO_2 captors at high temperatures, sodium metazirconate (Na_2ZrO_3) is among them [2–11].

There are different papers about Na_2ZrO_3 as CO_2 captor. Among them, it has been studied the particle size effect, demonstrating that Na_2ZrO_3 nanocrystals show high capture rates at low CO_2 partial pressures [12]. Also, it has been studied the CO_2 chemisorption kinetic process on Na_2ZrO_3, in that work it was estimated the CO_2 chemisorption and sodium diffusion activation energies [13]. On the other hand, the water vapor effect was evaluated during the CO_2 chemisorption process in Na_2ZrO_3, at low temperatures. The results showed that Na_2ZrO_3 presents better CO_2 chemisorption efficiencies in the presence of water vapor [14]. A recent paper used Na_2ZrO_3 as a model to explain the microstructural evolution of the carbonate interface formed (Na_2CO_3–ZrO_2) after the CO_2 chemisorption process. These results helped to better understand CO_2 chemisorption mechanism [15]. Also, the Na_2ZrO_3 must satisfy different general characteristics. One of these characteristics is related to the thermal stability and chemisorption–desorption regeneration process. About this specific issue, there are only two papers related to Na_2ZrO_3 regeneration; these studies only showed two and eight cycles at different thermal conditions [2,12]. In one case, the chemisorption was produced at 600 °C while desorption was at 780 °C, for 1 h each [2]. Besides, Zhao et al.[12] performed the eight cycles of chemisorption–desorption at 575 and 680 °C, respectively. In that case, after eight cycles, Na_2ZrO_3 seemed to present a good stability, having efficiencies of ~65%. In both cases, the CO_2 flow was equal or higher than 100 mL/min, which according to previous results imply a saturated solid–gas interface [16,17]. However, as it can be seen these information are not enough to determine the regeneration capacity, thermal stability and the best thermal conditions of the capture Na_2ZrO_3–CO_2 system. Therefore, the aim of the present work was to evaluate the CO_2 chemisorption–desorption regeneration capacity of Na_2ZrO_3 at different temperatures, giving special attention to the microstructural and kinetic changes produced in the ceramic, in order to determine the best thermal conditions of the CO_2 chemisorption in Na_2ZrO_3.

2. Experimental section

Na_2ZrO_3 was synthesized using a solid-state reaction that employed sodium carbonate (Na_2CO_3, Aldrich) and zirconium

* Corresponding author. Fax: +52 55 5616 1371.
E-mail address: pfeiffer@iim.unam.mx (H. Pfeiffer).

0022-4596/$ - see front matter © 2013 Elsevier Inc. All rights reserved.
http://dx.doi.org/10.1016/j.jssc.2013.06.014

oxide (ZrO_2, Aldrich). The powders were mechanically mixed and heat-treated at 850 °C for 6 h. To obtain pure Na_2ZrO_3, 20 wt% excess of sodium carbonate was used. The ceramic structural and microstructural properties were analyzed. While the correct structure was corroborated by XRD, the textural properties were determined by the N_2 adsorption, where the sample surface area was equal to 3.1 m^2/g (data not shown). The CO_2 cyclic chemisorption–desorption experiments were performed using a Q500HR instrument (TA Instruments). Samples were initially heated to the specific experimental temperature (between 500 and 800 °C) under a N_2 flow (Praxair, grade 4.8). After the sample reached the corresponding temperature, the gas flow was switched from N_2 to CO_2 (Praxair, grade 3.0), in order to perform the first CO_2 chemisorption process during 30 min. After the CO_2 chemisorption, the gas flow was switched to N_2 again, and the temperature was fitted to different desorption temperatures (700, 750 or 800 °C). As the desorption process implied different heating and cooling processes, the total desorption time varied between 30 and 45 min approximately in each case. In all the cases the experiments were performed using a total gas flow rate of 60 mL/min of N_2 or CO_2 throughout 20 cycles. Then, to elucidate the Na_2ZrO_3 stability after the cyclic performance, the Na_2ZrO_3–CO_2 cyclic products were analyzed structurally and microstructurally by X-ray diffraction (XRD) and scanning electron microscopy (SEM), respectively. A diffractometer (Bruker AXS, D8 Advance) coupled to a copper anode X-ray tube was used to identify the phases obtained after the cyclic experiments. The microstructural evolution of the Na_2ZrO_3 sample was analyzed by SEM on a JEOL JMS-7600F equipment. Finally, different kinetic analyses were performed in the cyclic chemisorption curves.

3. Results and discussion

It has been reported that Na_2ZrO_3 is able to trap, chemically, CO_2 according to the following reaction [12–15]:

$$Na_2ZrO_3+CO_2 \rightarrow Na_2CO_3+ZrO_2 \quad (1)$$

where the theoretical maximum weight increment determined by TG experiments would be 23.7 wt% (100% of efficiency). This weight increment corresponds to the weight gained by 1 mol of CO_2 chemisorbed in 1 mol of Na_2ZrO_3. Additionally, it must be mentioned that Na_2ZrO_3 melts at $T > 1000$ °C [18]. Thus, as different experiments were performed at temperatures equal or lower than 800 °C, there was not any fusion interference.

Base on the previous reaction model, twenty CO_2 chemisorption–desorption cycles were performed in Na_2ZrO_3 at different chemisorption temperatures (500–800 °C), but all desorption processes were produced at 800 °C, in order to guarantee the CO_2 desorption. If the desorption processes were produced at lower temperatures, the CO_2 desorbed decreased importantly (data not shown). Fig. 1 shows the curves produced at each temperature. At 500 °C, all the cycles seemed to be very similar, reaching weight increments of about 17 wt% which corresponded to an efficiency of 71.7%. When the cyclic experiment was performed at 550 °C, the efficiency was increased up to 80.2%. Additionally, at this temperature (550 °C) the equilibrium was not reached in the first five cycles, although after the sixth cycle the chemisorption process did reach the equilibrium. Similar efficiencies (~75–80%) and equilibrium behaviors were observed at 600 and 700 °C. Finally, at 800 °C the efficiency tended to decrease as a function of the cycles. In the first cycle the sample presented an efficiency of 91.9%, but it decreased to only 58.2% after 20 cycles. All these results are summarized in Fig. 2, where the maximum weight increments observed in each cycle were plotted. At the highest temperature (800 °C), it must be established that CO_2 capture seemed to be related to incomplete desorption processes. Another probable explanation to the decrease of chemisorption after several cycles at this specific temperature may be associated to sample microstructural changes.

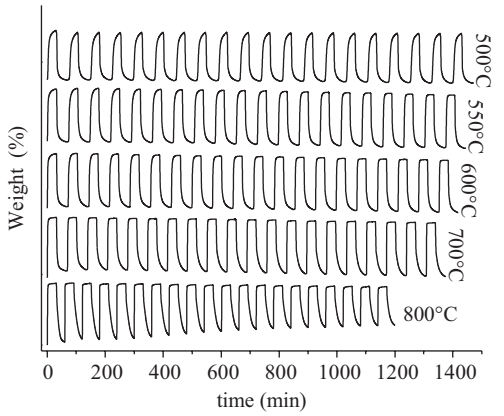

Fig. 1. Multicyclic performance of CO_2 chemisorption–desorption on Na_2ZrO_3–CO_2 chemisorptions were performed at different temperatures between 500 and 800 °C for 30 min, while desorption processes were performed at 800 °C, for all the cases, over 30 min into a N_2 flux.

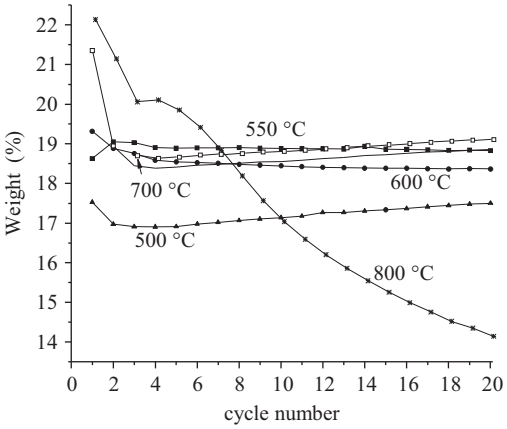

Fig. 2. Maximum experimental weight increments determined after each CO_2 chemisorption process in Na_2ZrO_3 multicyclic curves at the different temperatures.

Desorption process was performed at 800 °C, independently of the CO_2 chemisorption temperature. Nevertheless, the desorption trends observed in the Fig. 1 seem to be faster at the lowest temperatures. At 500 and 550 °C, the total desorption occurred in about 12–15 min, but the desorption time was incremented as a function of the CO_2 chemisorption temperature. In fact, at 800 °C the desorption process could not be completed. Therefore, in order to analyze if the desorption time was responsible for the CO_2 capture efficiency decrement a second cycle experiment was performed at 800 °C, but in this case the desorption time was larger, 60 min. As it can be seen in Fig. 3, larger desorption times produced better CO_2 capture efficiencies, although the efficient decrement continued as a function of the cycle numbers. This result indicates some Na_2ZrO_3 degradation at high temperatures. Perhaps part of the sodium atoms are sublimating.

Moreover, it was recently published that the alkaline external shell produced during the CO_2 chemisorption produced in Na_2ZrO_3 presents different microstructural characteristics depending on the temperature [15]. It was shown that the Na_2CO_3–ZrO_2 external shell produced during the CO_2 capture on Na_2ZrO_3 at $T \leq 550$ °C is mesoporous. Thus, under these thermal conditions, the CO_2 chemisorption and desorption processes must not be limited.

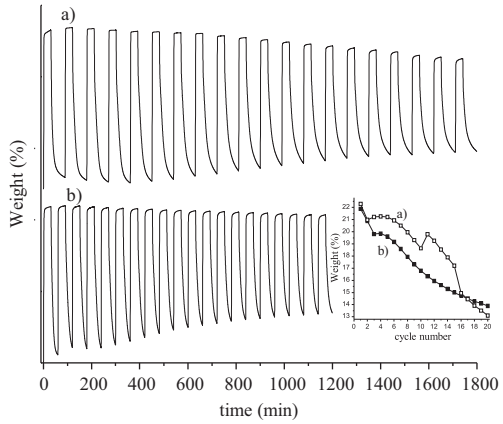

Fig. 3. Multicyclic performance of CO_2 chemisorption–desorption on Na_2ZrO_3, where the CO_2 chemisorptions were performed at 800 °C for 60 (a) or 30 min (b). The inset square shows the experimental weight increments determined under these specific conditions.

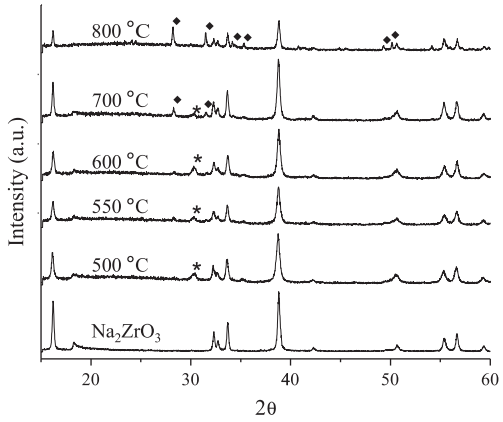

Fig. 4. XRD patterns of Na_2ZrO_3 after 20 cycles of CO_2 chemisorption-desorption. The peaks labeled correspond to different ZrO_2 phases: (♦) monoclinic and (*) cubic or tetragonal. All the other peaks correspond to Na_2ZrO_3.

In other words, CO_2 chemisorption and desorption processes are favored at $T \leq 550$ °C, as the CO_2 molecules can diffuse throughout the Na_2CO_3–ZrO_2 mesoporous external shell, while at higher temperatures the same two processes are limited to inter-crystalline diffusion processes. Results obtained here are in total agreement with that paper, as the best cyclic behavior was observed at 550 °C. At 600 and 700 °C the cyclic behaviors were slightly smaller due to the inter-crystalline diffusion processes.

Additionally, in order to corroborate the differences described above, the Na_2ZrO_3 cycled products were further analyzed by XRD and SEM. Fig. 4 shows the XRD patterns of the initial Na_2ZrO_3 sample and the final powders obtained after the 20 cycles at each temperature. As it can be seen, although the Na_2ZrO_3 phase is present in all the cyclic sample products, the XRD patterns presented some specific variations as a function of the temperature. In fact, different ZrO_2 phases could be determined as a function of the cyclic temperature. The XRD patterns of the samples treated between 500 and 600 °C presented a wide peak at 30.3°, which may be associated to the cubic or tetragonal ZrO_2 phases [19]. The presence of any of these metastable phases can be explained by their stabilization produced in the mixed external shell composed by ZrO_2 and Na_2ZrO_3. The last occurs by the mechanical constrainment of the zirconia particles by the surrounding matrix, on the basis of Garvie's hypothesis [20–22]. Another option may be the Na-doped ZrO_2 phase formation, as it was recently reported by Näfe and Karpukhina [18]. Furthermore, the XRD patterns of the 700 and 800 °C sample products clearly showed the presence of the monoclinic ZrO_2 phase. All these results indicate the partial decomposition of the sodium zirconate phase. This result is in very good agreement with the CO_2 cyclic chemisorption decrement observed at 800 °C, which indicates that CO_2 chemisorption–desorption processes are limited due to microstructural factors as explained before, but by structural changes as well.

To continue with the cyclic products characterization, the samples treated at different temperatures were analyzed by SEM. Fig. 5 shows the SEM images of the original Na_2ZrO_3, the sample after 30 min of CO_2 chemisorption and after 20 chemisorption–desorption cycles. Original Na_2ZrO_3 particles had a dense polyhedral morphology with particle sizes between 100 and 500 nm (Fig. 5a and b). These particles produced agglomerates. After the carbonation process (Fig. 5c and d) the sample morphology did not seem to change significantly. However, the presence of two different phases was determined by the particle contrasts observed in the corresponding backscattered electron images (BSEI). These two phases must correspond to Na_2CO_3 and ZrO_2, because they are the Na_2ZrO_3 carbonation products. Thus, the contrast differences arise from the differences in mean atomic number ($\overline{Z}$) of Na_2CO_3 and ZrO_2, 8.666 and 18.666, respectively. Therefore, the backscattered electron coefficient (η) [23] of these phases increases from 0.0999 to 0.2145 for Na_2CO_3 (dark phase) and ZrO_2 (light phase), respectively. After 20 CO_2 chemisorption–desorption cycles, the Na_2ZrO_3 morphology presented some minor changes (Fig. 5e and f). Again, the particle size did not seem to change, but the Na_2ZrO_3 particles seemed to be partially sintered and the surface presented some kind of texture. These process may be produced due to the CO_2 chemisorption–desorption processes, which implied a continuous atom movement, enhanced by the desorption temperature, 800 °C. Additionally, Fig. 5e presents some visual contrast, which may be attributed to the presence of some Na_2CO_3 after the 20 cycles or the partial Na_2ZrO_3 decomposition.

When the CO_2 capture process was performed at higher temperatures than 500 °C the final Na_2ZrO_3 morphology tended to change (Fig. 6), and of course it had a noticeable effect on the Na_2ZrO_3 material after the 20 cycles (Fig. 7). After the carbonation process, it was observed the presence of the two different phases previously attributed to Na_2CO_3 and ZrO_2 formations, independently of the chemisorption temperature (Fig. 6). Nevertheless, the particle morphology of the resulting particles changed. Samples treated at 550 and 600 °C presented some evident particle fragmentation, which was increased as a function of temperature (Fig. 6a and b). If the chemisorption process was produced at 700 °C, the particle fragmentation evolved to form new very tiny particles of around 15 nm. Finally, at 800 °C these tiny particles increased their size up to 100–200 nm. This microstructural evolution can be explained by the Na_2CO_3–ZrO_2 porous phase formation reported previously and described above [15].

As it could be expected the microstructural changes observed after the CO_2 chemisorption process, produced important changes in the final Na_2ZrO_3 particles after 20 cycles (Fig. 7). At 550 and 600 °C (Fig. 7a and b), where some fragmentation had been observed during the first CO_2 chemisorption, it was possible to observe some small and polyhedral particles (~150 nm) sintered and produced macroporous agglomerates. Thus, the initial Na_2ZrO_3 fragmentation progress to this small and sintered particles. Then, at higher temperatures (700 and 800 °C, Fig. 7c and d) the particles tended to grow becoming in a denser agglomerates. Something else must be pointed out, the images present some contrast (as it was seen at 500 °C), which had been attributed to a partial Na_2CO_3 presence and Na_2ZrO_3 decomposition. In fact the closer images (left size of the Fig. 7) show that particles have some

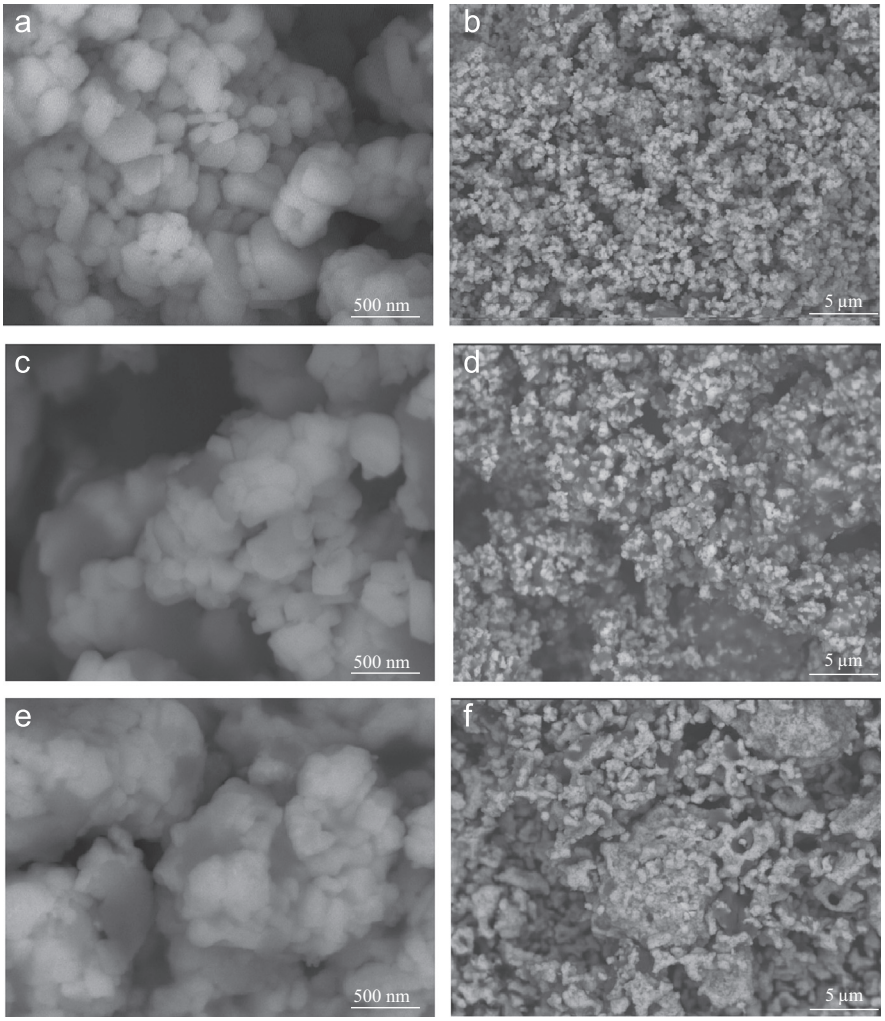

Fig. 5. SEM images of the original Na_2ZrO_3 (a and b), Na_2ZrO_3 after 30 min of carbonation (c and d) and Na_2ZrO_3 after 20 cycles (e and f).

small bright areas, which may be attributed to the ZrO_2 formation detected by the XRD experiments described above.

After the structural and microstructural characterizations, the cyclic behavior was analyzed kinetically. In that sense, different models have been used to determine some kinetic parameters of the CO_2 capture process in alkaline ceramics such as Li_4SiO_4, Li_2ZrO_3, Li_5AlO_4 and Na_2ZrO_3 [8,13,24,25]. Assuming that there are two global processes taking place during CO_2 capture on Na_3ZrO_3 (CO_2 direct chemisorption and CO_2 chemisorption controlled by diffusion processes [8,13]), some of the cyclic isotherms (cycles number 1, 5, 10 and 20) were fitted to a double exponential model.

$$y = A\exp^{-k_1 t} + B\exp^{-k_2 t} + C \quad (2)$$

where y represents the mass of CO_2 chemisorbed, t is the time, and k_1 and k_2 are the exponential constants for the CO_2 direct chemisorption produced over the particles and the CO_2 chemisorption kinetically controlled by diffusion processes, respectively. Additionally, the pre-exponential factors A and B indicate the intervals at which each process controls the whole CO_2 capture process, and C indicates the y-intercept.

Table 1 shows the constant values obtained for the CO_2 direct chemisorption (k_1) and the chemisorption kinetically controlled by diffusion processes (k_2), including the pre-exponential constants and R^2 values for the cycle numbers 1, 5, 10 and 20 of each thermal condition. As it can be seen, the k_1 values obtained, independently of the cycle number of temperature, are always one order of magnitude higher than those obtained for the k_2 constants, at least. Additionally, it must be mentioned that these values are in good agreement with previous reports [13,16]. So, the CO_2 chemisorption controlled by diffusion processes is the limiting step of the whole reaction process. If the k constant values are analyzed as a function of the chemisorption temperature, both constants tend to increase when the temperature was increased as well, as it could be expected.

Additionally, at each temperature the k_1 and k_2 values are considerably similar after the 20 cycles, showing a high kinetic stability. k values did not present significant variation after 20 cycles at any temperature, although the CO_2 capture was importantly decreased at high temperatures, specifically at 800 °C (see Fig. 2). To explain this behavior, it must be considered the formation of different ZrO_2 phases, which implies that sodium must be partially lost, perhaps by sublimation. Therefore, if a part of the reactive sodium is being lost, the final CO_2 chemisorption capacity must be decreased, independently of the kinetic factors.

4. Conclusions

Different Na_2ZrO_3–CO_2 cyclic experiments were evaluated in order to determine structural, microstructural and kinetic variations, and consequently the possible cyclic utilization of Na_2ZrO_3 as CO_2 captor. CO_2 chemisorption–desorption experiments performed between 500 and 700 °C presented good cyclic behaviors

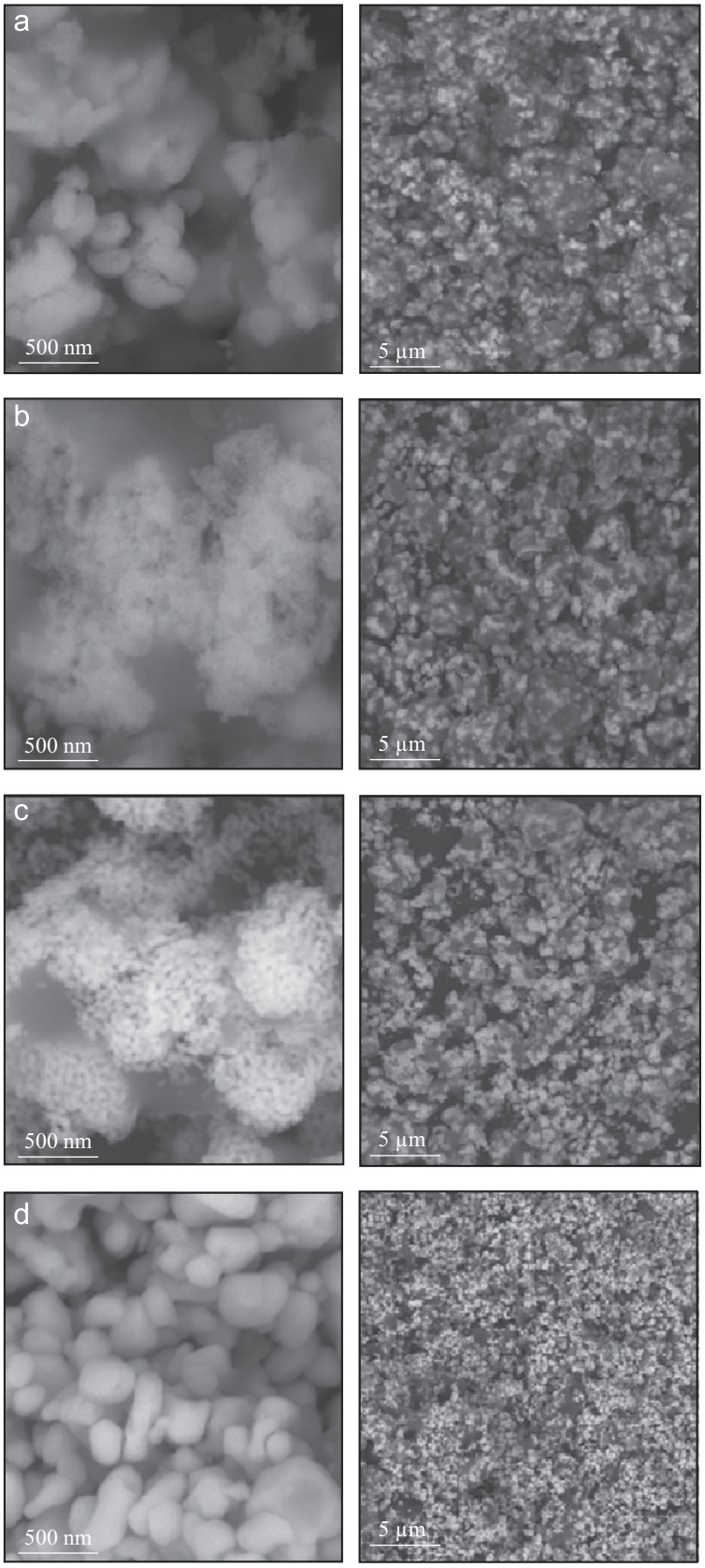

Fig. 6. SEM images of Na_2ZrO_3 after the carbonation process performed at different temperatures a) 550 °C, b) 600 °C, c) 700°C and d) 800 °C.

during 20 cycles. These results are very important as the combustion gases are usually eliminated in similar temperature ranges. As it was expected, from previous reports, the sample treated at 550 °C presented the highest CO_2 chemisorptions. It has been explained in terms of the Na_2CO_3–ZrO_2 microstructural characteristics produced at this temperature conditions. On the contrary,

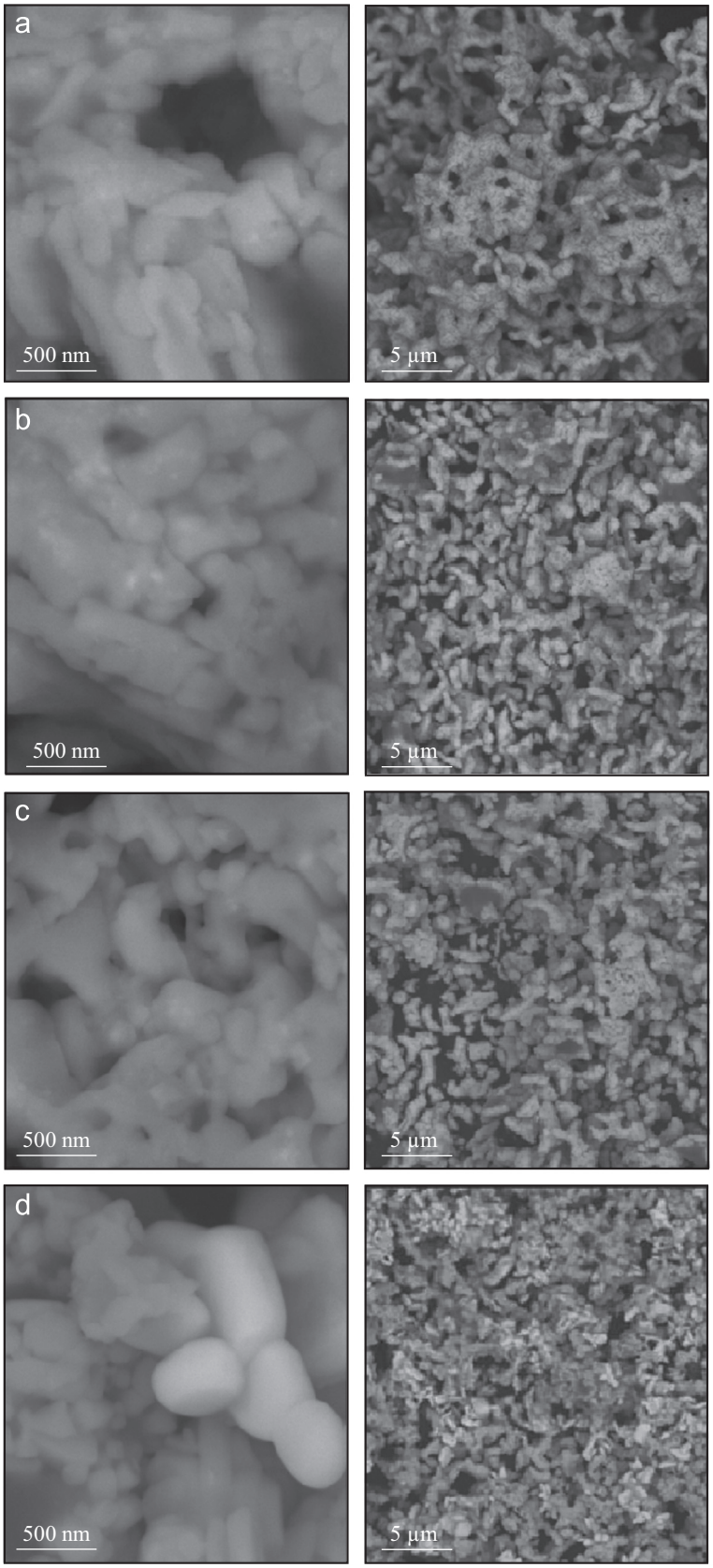

Fig. 7. SEM images of Na_2ZrO_3 after 20 cycles of CO_2 chemisorption–desorption at different temperatures a) 550 °C, b) 600 °C, c) 700°C and d) 800 °C.

when the Na_2ZrO_3 sample was treated at 800 °C, the first two cycles presented better CO_2 chemisorptions than any other temperatures. However, the CO_2 chemisorption was decreased dramatically from the third to the twentieth cycles. Something else has to be pointed out, the desorption process had to be performed at $T > 800$ °C.

Table 1
CO_2 chemisorption kinetic parameters obtained for the Na_2ZrO_3 after different cycles and temperatures.

Temperature (°C)	Cycle number	k_1 (s^{-1})	k_2 (s^{-1})	A	B	C	R^2
500	1	0.00623	0.00073	−15.1123	−3.9054	117.5171	0.9969
	5	0.00523	0.00047	−12.8723	−6.0464	117.8479	0.9979
	10	0.00459	0.00056	−14.5492	−4.1231	117.2968	0.9966
	20	0.00534	0.00031	−10.8642	−5.9755	116.4249	0.9995
550	1	0.01073	0.00114	−17.1651	−3.1527	118.2559	0.9948
	5	0.00792	0.00129	−16.8818	−3.4697	118.5833	0.9967
	10	0.00846	0.00162	−18.2749	−1.7754	118.1870	0.9961
	20	0.01012	0.00107	−16.9587	−0.0342	116.0075	0.9980
600	1	0.01573	0.00151	−18.0041	−2.8391	118.8239	0.9945
	5	0.0165	0.00376	−13.6549	−5.1346	117.5001	0.9979
	10	0.01383	0.00271	−18.9765	−1.4444	118.0350	0.9931
	20	0.01903	0.00124	−17.4834	−0.2448	116.3918	0.9968
700	1	0.02814	0.00389	−20.0592	−2.2439	120.5139	0.9947
	5	0.02401	0.00521	−16.9813	−1.47	117.0076	0.9964
	10	0.02749	0.00199	−18.3816	−0.3041	116.9669	0.9941
	20	0.03387	0.00415	−18.8931	−0.2135	117.1004	0.9852
800	1	0.02827	0.00195	−23.2548	−0.6201	121.1535	0.9914
	5	0.03819	0.00165	−20.9270	−0.2985	118.0068	0.967
	10	0.03319	0.00179	−17.6762	−0.1959	115.2652	0.9743
	20	0.03135	0.00107	−13.6109	−0.5854	112.4780	0.9866

It was determined, by XRD, a partial Na_2ZrO_3 decomposition as different ZrO_2 phases were determined after 20 cycles. While, between 500 and 600 °C a cubic or tetragonal ZrO_2 phase was observed, and at $T > 600$ °C the monoclinic ZrO_2 was found. The presence of these phases must be associated to sodium sublimation, which may be produced during the cyclic desorption processes. Additionally, a Na_2ZrO_3 microstructural analysis showed a systematic morphological evolution. It seems that initially the original Na_2ZrO_3 particles are fractured due to the volume expansion generated by the Na_2CO_3 formation. Then, after several cycles this tiny fractured particles tend to sinter producing new polyhedral Na_2ZrO_3–ZrO_2 particles. Finally, the kinetic analysis showed a high stability of the CO_2 chemisorption reaction in the whole temperature range of analysis. In conclusion, it could be said that Na_2ZrO_3 presents very good CO_2 cyclic capture properties, which may be extrapolated to the industry and different technologies.

Acknowledgments

This work was financially supported by the projects SENER-CONACYT 150358 and PAPIIT-UNAM 102313. L. Martínez-dlCruz thanks CONACYT for financial support and the authors thank to A. Tejeda, G. González-Mancera and O. Novelo for the technical help.

References

[1] S. Wang, C. An, Q. Zhang, J. Mater. Chem. A 1 (2013) 3540–3550.
[2] M. Kato, S. Yoshikawa, K. Nakagawa, J. Mater. Sci. Lett. 21 (2002) 485–487.
[3] A. López-Ortiz, N.G. Perez-Rivera, A. Reyes-Rojas, D. Lardizabal-Gutierrez, Sep. Sci. Technol. 39 (2004) 3559–3572.
[4] H. Pfeiffer, P. Bosch, Chem. Mater. 17 (2005) 1704–1710.
[5] M. Kato, K. Essaki, K. Nakagawa, Y. Suyama, K. Terasaka, J. Ceram. Soc. Jpn. 113 (2005) 684–686.
[6] N. Togashi, T. Okumura, K. Oh-ishi, J. Ceram. Soc. Jpn. 115 (2007) 324–328.
[7] L.M. Palacios-Romero, H. Pfeiffer, Chem. Lett. 37 (2008) 862–863.
[8] T.L. Ávalos-Rendón, J. Casa-Madrid, H. Pfeiffer, J. Phys. Chem. A 113 (2009) 6919–6923.
[9] J. Ortiz-Landeros, C. Gómez-Yáñez, H. Pfeiffer, J. Solid State Chem. 184 (2011) 2257–2262.
[10] M. Khokhani, R.B. Khomane, B.D. Kulkarni, J. Sol–Gel Sci. Technol. 61 (2012) 316–320.
[11] M. Olivares-Marín, M. Maroto-Valer, Greenhouse Gas Sci. Technol. 2 (2012) 20–35.
[12] T. Zhao, E. Ochoa-Fernández, M. Rønning, D. Chen, Chem. Mater. 19 (2007) 3294–3301.
[13] I. Alcérreca-Corte, E. Fregoso-Israel, H. Pfeiffer, J. Phys. Chem. C 112 (2008) 6520–6525.
[14] G.G. Santillán-Reyes, H. Pfeiffer, Int. J. Greenhouse Gas Control 5 (2011) 1624–1629.
[15] L. Martínez-dlCruz, H. Pfeiffer, J. Phys. Chem. C 116 (2012) 9675–9680.
[16] R. Rodríguez-Mosqueda, H. Pfeiffer, J. Phys. Chem. A 114 (2010) 4535–4541.
[17] R. Xiong, J. Ida, Y.S. Lin, Chem. Eng. Sci. 58 (2003) 4377–4385.
[18] H. Näfe, N. Karpukhina, J. Am. Ceram. Soc. 90 (2007) 1597–1602.
[19] M.T. Colomer, M. Maczka., J. Solid State Chem. 184 (2011) 365–372.
[20] F. Monte, W. Larsen, J.D. Mackenzie, J. Am. Ceram. Soc. 83 (2000) 628–634.
[21] Y. Murase, E. Kato, K. Daimon, J. Am. Ceram. Soc. 69 (1986) 83–87.
[22] J. Wang, R. Raj, J. Am. Ceram. Soc. 74 (1991) 1707–1709.
[23] J.I. Goldstein, D.E. Newbury, P. Echlin, D.C. Joy, C. Fiori, E. Lifshin, Scanning Electron Microscopy and X-ray Microanalysis, Plenum, New York, 1981.
[24] Q. Zhang, D. Han, Y. Liu, Q. Ye, Z. Zhu, AIChE J. 59 (2013) 901–911.
[25] X.S. Yin, Q.H. Zhang, J.G. Yu, Inorg. Chem. 50 (2011) 2844–2850.